Digital Demodulator of the Quadrature Amplitude Modulation Signals

Oleg Chernoyarov[1,2,3], Alexey Glushkov[4], Vladimir Litvinenko[5], Yuliya Litvinenko[5], Boris Matveev[5]

[1]*International Laboratory of Statistics of Stochastic Processes and Quantitative Finance, National Research Tomsk State University, Lenin Avenue, 36, 634050, Tomsk, Russia*
[2]*Department of Higher Mathematics and System Analysis, Faculty of Engineering and Economics, Maikop State Technological University, Pervomayskaya st. 191, 385000, Maikop, Russia*
[3]*Department of Electronics and Nanoelectronics, Faculty of Electrical Engineering, National Research University "MPEI", Krasnokazarmennaya st., 14, 111250, Moscow, Russia, chernoyarovov@mpei.ru*
[4]*Department of Infocommunication Systems and Technologies, Faculty of Radio Engineering, Voronezh Institute of the Ministry of Internal Affairs of the Russian Federation, Patriotov Avenue, 53, 394065, Voronezh, Russia*
[5]*Department of Radio Engineering, Faculty of Radio Engineering and Electronics, Voronezh State Technical University, Moscow Avenue, 14, 394026, Voronezh, Russia*

In this paper, the digital algorithm and the device for the demodulation of the quadrature amplitude modulation signals are considered. The fundamental advantages of our approach are simple hardware implementation, minimal number of arithmetic operations required over the signal period as well as the potential interference immunity in the presence of Gaussian noise. The expressions have been found for the error probability and their inaccuracy has been estimated. By means of the statistical simulation methods, the practical interference immunity of the introduced demodulator, together with the influence of phase locking errors have been tested. The introduced demodulator can be implemented either as a device independent from the programmable logic devices, or as an installation unit of the receiver equipment.

Keywords: Quadrature amplitude modulation, coherent signal processing, noise interference, interference immunity, phase locking.

1. INTRODUCTION

Quadrature amplitude modulation (QAM) is widely used in systems for transmitting discrete multilocation signals via wire and radio channels [1]-[3] because QAM provides high-speed data transfer together with spectral efficiency [1]. However, the common QAM signal demodulation devices have a few disadvantages. The first one is the use of analog signal processing requiring compensation of both the quadrature channels amplitude difference and some other errors [4], [5]. Another is the complexity of the signal processing digital implementation involving a large number of arithmetic operations to deal with each of the received signal samples that implies the need for an expensive high-speed hardware [6], [7].

It is noteworthy that the adaptive algorithms have been developed for the QAM signal demodulation in varied data transmission systems [8]-[10]. However, in this case, their implementation may require significant computational resources.

In this paper, built based on the fast-digital algorithm for optimal processing of the narrow-band signals [11], [12], the simple digital high-frequency QAM demodulator is introduced that has none of the disadvantages mentioned above and that can be efficiently implemented by means of modern programmable logic devices (PLDs).

2. THE ALGORITHM FOR QAM SIGNAL DEMODULATION

The high-frequency QAM signal (for example, from the intermediate frequency section output of the receiver) takes the form of

$$s(t) = A(t)\cos \omega_0 t + B(t)\sin \omega_0 t , \qquad (1)$$

where $A(t)$ and $B(t)$ are the amplitudes of its in-phase and quadrature components taking the discrete values according to the modulating digital signal; $\omega_0 = 2\pi f_0$ and f_0 is carrier frequency. For example, while forming the sixteen position QAM signal (16 QAM), the transferred four-bit

binary code is divided into two two-bit combinations 00, 01, 10, and 11 under which the amplitudes $A(t)$ or $B(t)$ take the values independently from each other, for example, $-3U$, $-U$, U, and $3U$ correspondingly (where U is the specified value). The normalized time diagrams $A(t)$, $B(t)$, and $s(t)$ are drawn in Fig.1. The information symbol duration is $\tau = NT$, where $T = 1/f_0$ is the carrier period, $N = 2^n$ is the number of periods, n is an integer.

a)

b)
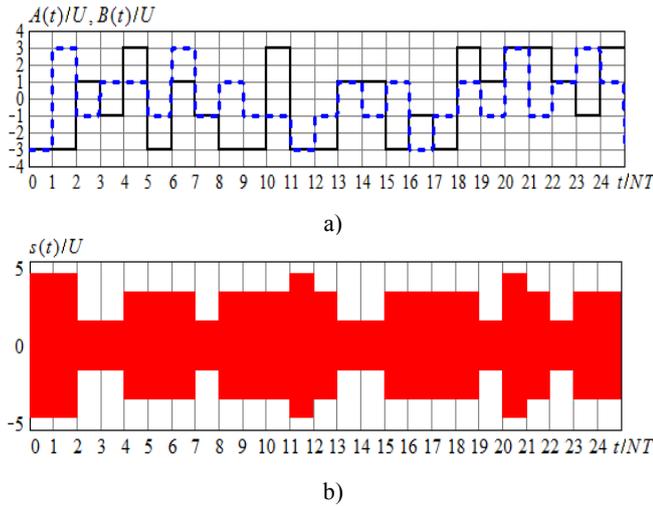
Fig.1. The time diagrams of the amplitudes of the in-phase and the quadrature components a) and of the QAM signal b).

The values of the amplitudes of the in-phase and quadrature components are represented by the points on the plane (A, B) in the signal diagram called "constellation".

The block diagram of the QAM signal demodulator is shown in Fig.2. The input signal $s(t)$ (1) is passed to the input of the analog-to-digital converter (ADC) operated by the clock generator (CG) with the frequency $f_Q = 4f_0$. As a result, the four samples s_{i0}, s_{i1}, s_{i2}, s_{i3} are formed over each of the i-th signal period.
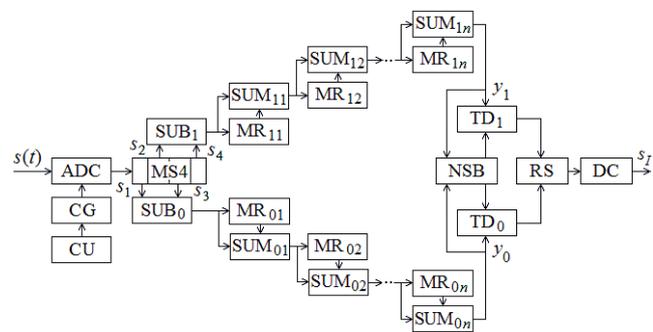
Fig.2. The block diagram of the QAM signal demodulator.

The synchronism between the CG and the received signal is provided by the clock unit (CU) implemented, for example, according to [13]. The received samples are stored

in the multibit shifter (MS4) containing four samples. After that, the fast-computational procedure [11], [12] of the accumulation of quadrature channel sample differences $(s_{i2} - s_{i0})$ and $(s_{i3} - s_{i1})$ over the last N periods is defined by the expressions

$$y_{i0} = \sum_{j=0}^{N-1} \left[s_{(i-j)2} - s_{(i-j)0} \right], \qquad (2)$$

$$y_{i1} = \sum_{j=0}^{N-1} \left[s_{(i-j)3} - s_{(i-j)1} \right]. \qquad (3)$$

In the subtractors SUB_0 and SUB_1, the differences are determined of even and odd samples which are then summarized with the contents of the multibit registers MR_{01} and MR_{11}. Each of these registers contains one value of each of the differences obtained while processing the previous period. Thus, the sums of differences of the samples of the two neighboring periods are formed. Thereafter, new values of the samples' differences are poked into MR_{01} and MR_{11} registers substituting their previous contents. Then, in the summators SUM_{01}/SUM_{11} and the multibit shifters MR_{02}/MR_{12}, the sums of the four neighboring samples' differences are calculated and stored. Further the device cycles are carried out likewise and, as a result, the responses y_{i0} (2) and y_{i1} (3) are generated at the outputs of the quadrature processing channels.

The values of the responses of the quadrature channels y_{i0} and y_{i1} are compared with the threshold levels (for 16 QAM, they are equal to 0 and $\pm 2U$) in the thresholders TD_0 and TD_1 at the moment of the symbol termination. Thus, in each channel the received information code is determined and the decision on the received symbol is made in the resolver RS and the decoder DC. Normalizing and synchronizing unit provides demodulator bit timing.

As in (2), (3) there is a large number of summation operations, the normalization of non-Gaussian interferences is carried out in the demodulator.

The considered device can be implemented based on the modern PLDs providing the QAM signal processing at the central frequency f_0 whose value may be up to several tens of megahertz.

3. THE SIMULATION OF THE QAM SIGNAL DEMODULATOR

In Fig.3.a) and Fig.3.b), we can see the normalized time diagrams of the responses of the quadrature channels $y_{i0}/2NU$ and $y_{i1}/2NU$ obtained by simulation in case when $N = 64$ and interferences are absent. Here by dotted lines the transmitted signals $A(t)/U$ and $B(t)/U$ are shown. The straight-line form of responses indicates that the demodulator provides optimal signal processing. The decisions on the received symbols are made at their termination while the values of i/N are the integers.

In Fig.4. the "constellations" of the normalized results of the QAM signal processing are presented in the absence of interference (Fig.4.a)) and in the presence of the band Gaussian interference (Fig.4.b)).

a)

b)
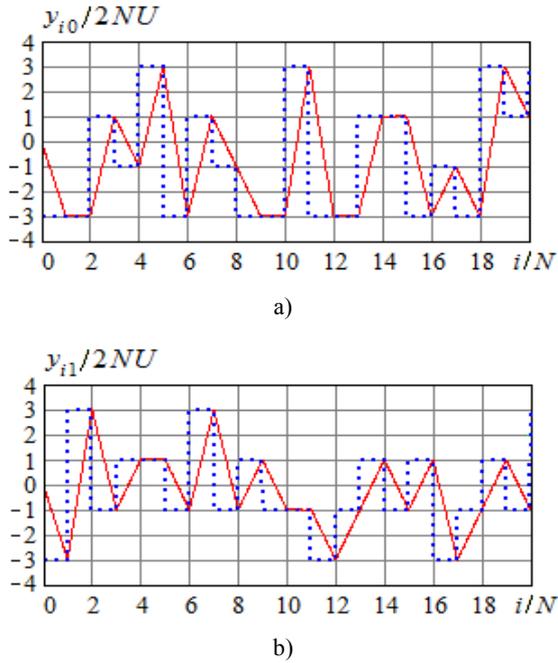
Fig.3. The responses of the quadrature channels.

a)

b)
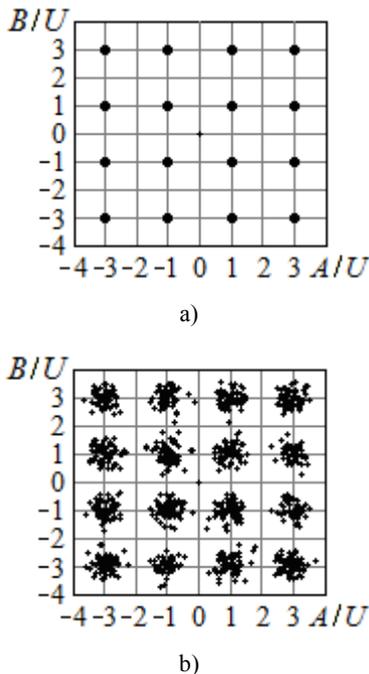
Fig.4. The 16 QAM signal "constellations" in the absence of interference a) and in the presence of the band Gaussian interference b).

The demodulator has effective frequency selective properties of its own. They can be estimated while passing the linear-frequency modulation (LFM) signal with the band

center f_0 and the unit amplitude to the demodulator input. The Δf location of the amplitude spectrum of such signal is shown in Fig.5.a) under $f_0 = 10$ MHz. Here $\Delta f = f - f_0$. In coherent processing, the responses of the quadrature channels y_{i0} and y_{i1} of the input harmonic signal depend not only on its frequency but also on its initial phase. In order to eliminate the initial phase influence, one can determine the value $z_i = \sqrt{y_{i0}^2 + y_{i1}^2}$ which does not depend on the input signal initial phase and is not less than the modules of each of the quadrature channel responses. In Fig.5.b), by solid line, the dependence is plotted of the normalized quadrature channel response upon the LFM signal frequency linearly increasing in time. It has been obtained by means of simulation under $N = 512$. Here, by dotted line, the normalized $z/2N$ value is also represented. In paper [12], the following expression is obtained for z as the function of the current frequency f:

$$z(f) = \left| \sin(N\pi f / f_0) / \cos(\pi f / 2f_0) \right|. \qquad (4)$$

We can see that the graph of $z = z(\Delta f)$ coincides with the dotted line in Fig.5.b).

a)

b)
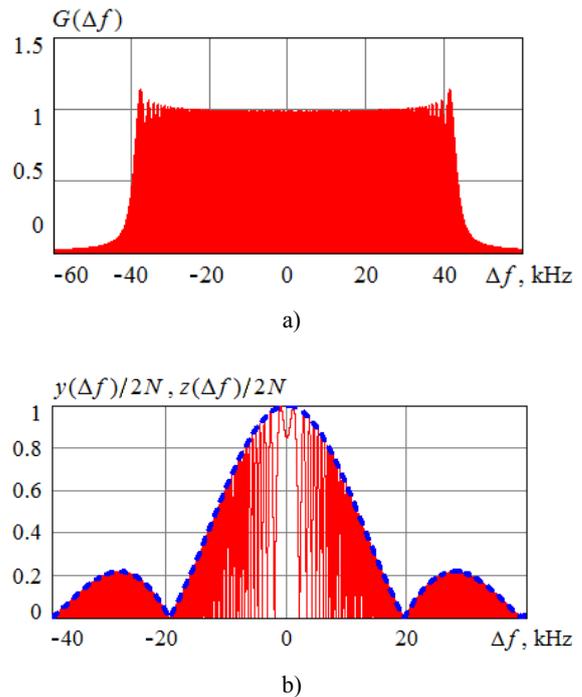
Fig.5. The linear-frequency modulation signal spectrum a) and the quadrature channel response b).

4. THE INTERFERENCE IMMUNITY OF THE QAM SIGNAL DEMODULATOR

For approximate estimation of the interference immunity of the QAM signal demodulator operating when the distortions of the useful signal are Gaussian, one determines the probability of transition of the transferring

"constellation" element to the neighboring values under the influence of interferences, as it is shown in Fig.6. If, at the receiving site, the coordinates of the transferred element in the center of the shaded rectangle do not extend beyond its borders, then the error has not occurred. Such an estimate of the probability of the correct reception will be understated for extreme rectangular areas.
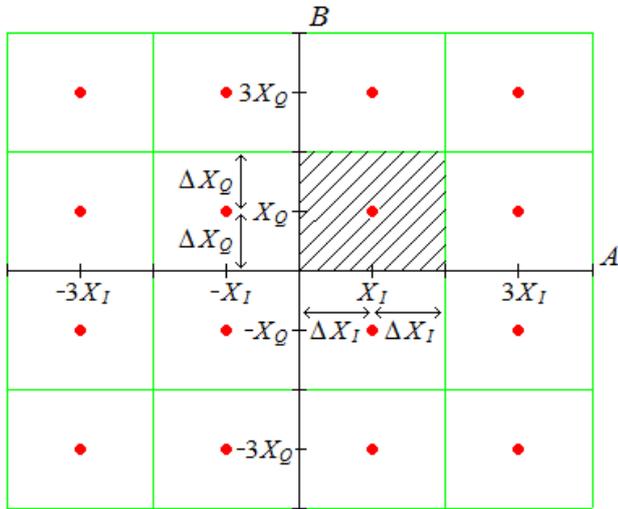
Fig.6. The explanation for the demodulation error situation.

In the algorithm under testing, no amplitude dissimilarity of the quadrature channels is present, as the signals corresponding to them are formed by the ADC based on the common input signal.

In each loop of the accumulation of the sample differences (Fig.2.) of the signals with the amplitudes S_I and S_Q that are in the in-phase and the quadrature channels, respectively, and are equal to $\pm U$ or $\pm 3U$ for 16 QAM, the responses' mean values X_I and X_Q over N periods are the following:

$$X_I = 2NS_I , \qquad X_Q = 2NS_Q . \tag{5}$$

As for the dispersions of the responses, they are the same and are equal to

$$\sigma^2 = 2N\sigma_n^2 . \tag{6}$$

Here σ_n^2 is the dispersion of the samples of the Gaussian noise at the input. For the sake of calculation simplicity, it is presupposed that these samples are statistically independent. The distance between the mean values of the neighboring positions in the demodulator responses (Fig.6.) is determined by the expression

$$2\Delta X = 4NU . \tag{7}$$

Taking into account (5) and (6), the two-dimensional probability density of the independent random Gaussian values x_I and x_Q of the responses of the quadrature channels y_0 and y_1, can be written as

$$w(x_I, x_Q) = \frac{1}{2\pi\sigma^2} \exp\left[-\frac{(x_I - X_I)^2 + (x_Q - X_Q)^2}{2\sigma^2} \right]. \tag{8}$$

If, in (8), one passes to the centered variables $x_0 = x_I - X_I$ and $x_1 = x_Q - X_Q$, then one can get

$$w(x_0, x_1) = \exp\left[-(x_0^2 + x_1^2)/2\sigma^2 \right]/2\pi\sigma^2 . \tag{9}$$

The variables x_0 and x_1 crossing the boundaries $\pm\Delta X$ will result in the error situation while determining the received position. Therefore, the error probability can be found as

$$p_{err} = 1 - \int_{-\Delta X}^{\Delta X} \int_{-\Delta X}^{\Delta X} w(x_0, x_1) dx_0 dx_1 =$$

$$= 1 - \frac{1}{2\pi\sigma^2} \int_{-\Delta X}^{\Delta X} \int_{-\Delta X}^{\Delta X} \exp\left(-\frac{x_0^2 + x_1^2}{2\sigma^2} \right) dx_0 dx_1 . \tag{10}$$

After simple transformations, it can be obtained

$$p_{err} = 1 - \left[1 - 2Q(\Delta X/\sigma) \right]^2 , \tag{11}$$

where $Q(x) = \int_x^{\infty} \exp(-u^2/2) du/\sqrt{2\pi}$ is Gaussian error integral [3]. In view of (6) and (7), the expression (11) can be transformed into

$$p_{err} = 1 - \left[1 - 2Q(\sqrt{2}h_0) \right]^2 . \tag{12}$$

Here

$$h_0 = \Delta X/\sigma\sqrt{2} = U\sqrt{N}/\sigma_n \tag{13}$$

is the voltage signal-to-noise ratio at the demodulator output, provided that the amplitude of the input signal in each of the quadrature channels is minimal (i.e., it is equal to U). In case of the four-position QAM, the formula (12) coincides with the common expression for the error probability for the four-position phase-shift keying (QPSK) [2], [3].

Equation (12) has been obtained without taking into account the exterior constellation domains. To estimate its accuracy, the error probability is determined in case of the four-position QAM. The corresponding constellation under $X_I = X_Q = U$ is shown in Fig. 7.
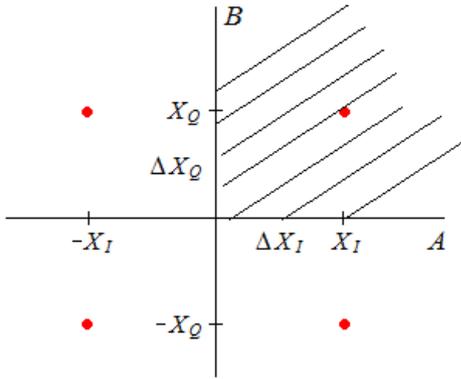
Fig.7. The four-position QAM constellation.

In this case, the error probability is equal to

$$p_{err4} = 1 - \int\limits_{-\Delta X}^{\infty} \int\limits_{-\Delta X}^{\infty} w(x_0, x_1) dx_0 dx_1 =$$

$$= 1 - \left[\frac{1}{\sqrt{2\pi}} \int\limits_{-\Delta X/\sigma}^{\infty} \exp\left(-\frac{y^2}{2}\right) dy \right]^2 . \qquad (14)$$

By applying (13) in (14), it can be obtained:

$$p_{err4} = 1 - Q^2\left(-\sqrt{2}h_0\right). \qquad (15)$$

Analogously, while receiving the binary phase-shift keyed signal, which can be considered as the QAM signal under $M = 2$, the well-known (see [1]-[3]) exact expression is obtained:

$$p_{err2} = 1 - \int\limits_{-\Delta X}^{\infty} w(x) dx =$$

$$= 1 - \frac{1}{\sqrt{2\pi}} \int\limits_{-\Delta X/\sigma}^{\infty} \exp\left(-\frac{y^2}{2}\right) dy = Q\left(\sqrt{2}h_0\right). \qquad (16)$$

In Fig.8., there can be seen the approximate dependence of the error probability $p_{err}(h_0)$ (12), as well as the exact curves $p_{err4}(h_0)$ (15) and $p_{err2}(h_0)$ (16). The upper solid line corresponds to the values of the error calculated by the formula (12), the lower solid line ($M = 4$) – to the ones calculated by the formula (15), and the dashed line ($M = 2$) – to those calculated by the formula (16). As it follows from Fig.8., even under the crudest estimation of the boundary constellation areas, the inaccuracy of the formula (12) is relatively small and it decreases rapidly with the rising M.

The most important characteristic of the demodulator is the operating signal-to-noise ratio h^2 that can be considered as the ratio of the signal power to the noise power [1]-[3]. The QAM signal amplitude (Fig.1.b)) changes together with the signal power and, thus, the signal-to-noise ratio. In [2], for the calculation of the demodulator characteristics, it is

suggested to use the mean values of the signal power by all the equiprobable signal versions. What is also introduced here is the power P_0 of the "base signal pulse" at the quadrature channel inputs having the minimum amplitude U and corresponding to the output signal-to-noise ratio h_0^2 (13).
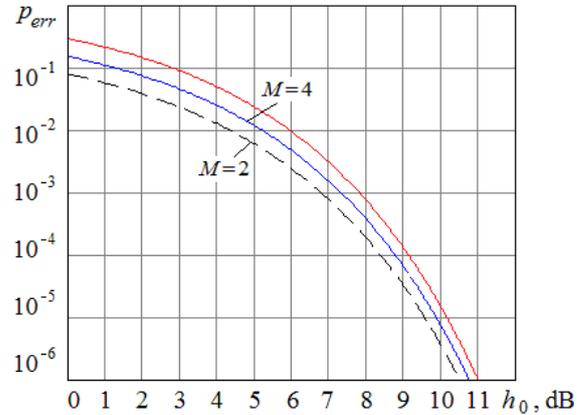
Fig.8. The dependences of the error probabilities upon the signal-to-noise ratio.

The signal element amplitudes in the quadrature channels are equal to $U_k = (2k-1)U$, $k = 1, 2, \ldots, K$, $K = \sqrt{M}/2$, while $P_k = (2k-1)^2 P_0$. As a result, P_{mean} denoting the power mean value of the equiprobable signals in the quadrature channels under M-position QAM with the constellation format presented in Fig.6. is equal to

$$P_{mean} = \frac{P_0}{K} \sum_{k=1}^{K} (2k-1)^2 = \frac{P_0}{K} \frac{K(2K-1)(2K+1)}{3} = \frac{M-1}{3} P_0 .$$

Then, for the mean signal-to-noise ratio, it is:

$$h^2 = (M-1)h_0^2/3 . \qquad (17)$$

Expressing the h value in terms of (17) and substituting it into (12) helps to obtain the expression for the error probability in the form of

$$p_{err} = 1 - \left[1 - 2Q\left(h\sqrt{6/(M-1)}\right)\right]^2 .$$

The same results are obtained in [2] while evaluating a potential interference immunity of the analog QAM signal demodulator. Therefore, the considered digital demodulation algorithm is optimal.

The dependences of p_{err} upon the time-averaged signal-to-noise ratio h in case of varied M are shown in Fig.9.

It is easy to see that the interference immunity of the QAM signal demodulation deteriorates if the number of M positions increases (the same results are presented in [1], [2] for analog demodulators). When $M = 4$, the QAM signal

corresponds to the four-position phase-shift keyed (QPSK) signal. At that, according to (15), $h = h_0$ while the corresponding curve in Fig.6. is described by the expression (12). That is, it represents the dependence of the error probability upon the signal-to-noise ratio h_0 for the basic signal pulse. Moreover, it corresponds to the upper solid line in Fig.8.
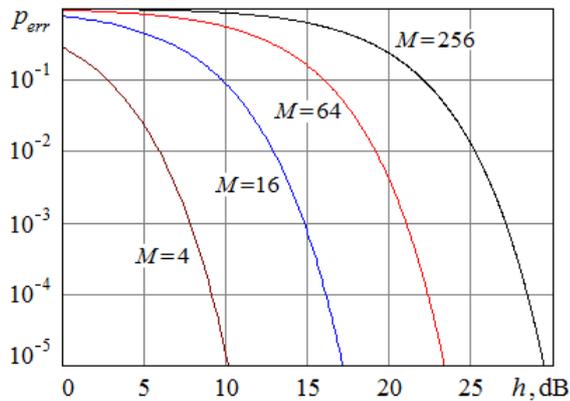
Fig.9. The error probability in case of demodulating the QAM signals of the varied formats.
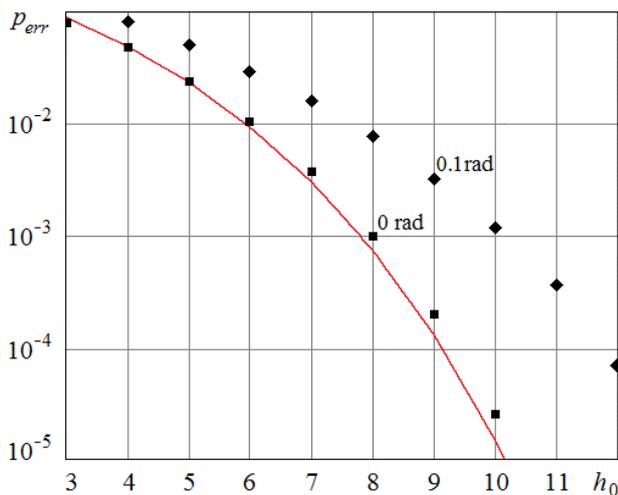
Fig.10. The simulation results of the digital 16 QAM signal demodulator.

In order to test the operability and performance of the presented demodulator, in Delphi and ISE WebPACK environments, the statistical simulation has been carried out of how it operates while receiving 16 QAM signals against the band Gaussian noise with the independent samples. In Fig.10., the dependences are shown of the error probability upon the signal-to-noise ratio h_0 in the absence of synchronizing errors and when $N = 64$ and $M = 16$. Here, by solid line, the error probability values calculated by the formula (12) are drawn while by squares – the corresponding simulation results. When obtaining the simulation results, the sample volume of the symbols being received has been chosen from 10^5 to 10^7, depending on

the signal-to-noise ratio. Thus, with the probability of 0.9, the confidence interval boundaries deviate from the values obtained during the simulation by no more than 10...15 %. It can be seen that the theoretical data correspond with the simulation data satisfactory under a wide range of h_0.

We have to emphasize that the performance of the coherent QAM signal demodulator depends primarily upon the accuracy of the phase locking of the ADC clock generator and the received signal. From [14], the estimates are known of the influence of the phase locking errors of the coherent binary phase-shift keyed signal demodulator upon the error probability. That study has demonstrated that the root-mean-square deviation of the input and the clock signal phase shifting should not exceed 0.1 rad.

When 16 QAM signal is received and the phase deviation between the clock and the input signals is constant and equal to 0.1 rad, the error probability increases significantly. This is illustrated by Fig.10. (rhombuses) for the case of $N = 64$ and $M = 16$. With increasing M, the interference immunity deteriorates abruptly. Thus, the requirements to the accuracy of the phase locking of the QAM signal demodulator are stricter than in the case of the coherent binary phase-shift keyed signal demodulation.

5. CONCLUSION

The introduced fast digital algorithm and the device for digital demodulation of the high-frequency QAM signals that is based on it require minimum number of computations over the signal period, and thus the hardware resources needed for their implementation are not too great. The demodulator has its own frequency selectivity, its frequency properties are matched with the received signal. The expressions for the probability of the inaccurate demodulation have been obtained and they show that the demodulator provides potential interference immunity against Gaussian noises. In the case of the non-Gaussian interferences, their normalization can often occur, and the demodulation algorithm can provide the optimal processing. As a result of the present study of the influence of the phase shifting between the received and the clock signals upon the error probability, it can be demonstrated that, for the multilocation QAM signals, the accuracy requirements to phase locking are higher than in binary signal demodulating. The considered demodulator can be effectively implemented by means of the modern PLDs, including, for example, the PLD Spartan-6 family (XC6SL25) produced by Xilinx [15]. These PLDs provide signal processing under $M = 16$ at the frequencies f_0 up to 50 MHz and with the required power of less than 80 mW. High-end PLD families allow processing the higher-frequency signals (up to $f_0 = 100 \div 150$ MHz) with higher values of M.

REFERENCES

[1] Feher, K. (1995). *Wireless Digital Communications: Modulation and Spread Spectrum Applications*. Prentice-Hall.

[2] Proakis, J., Salehi, M. (2007). *Digital Communications*. McGraw-Hill.

[3] Sklar, B. (2001). *Digital Communications: Fundamentals and Applications*. Prentice-Hall.

[4] Seguin, F., Lahuec, C., Lebert, J., Arzel, M., Jezequel, M. (2004). Analogue 16-QAM demodulator. *Electronics Letters*, 40 (18), 1138-1140.

[5] Sharma, R.H., Bhatt, K.R. (2015). A review on implementation of QAM on FPGA. *International Journal of Innovative Research in Computer and Communication Engineering*, 3 (3), 1684-1688.

[6] Naveen, K.B., Sree Rangaraju, M.N. (2016). Energy efficient QAM modulation/demodulation architecture using reversible logic gates. *International Journal of Scientific & Engineering Research*, 7 (8), 759-763.

[7] Ayat, M., Mirzakuchaki, S., Beheshti-Shirazi, A., (2016). Design and implementation of high throughput, robust, parallel M-QAM demodulator in digital communication receivers. *IEEE Transactions on Circuits and Systems I: Regular Papers*, 63 (8), 1295-1304.

[8] Yanxin, L., Aiqun, H. (2007). An adaptive demodulation method for QAM signals. In *IEEE 2007 International Symposium on Microwave, Antenna, Propagation, and EMC Technologies for Wireless Communications*, 16-17 August 2007, Hangzhou, China. IEEE, 1064-1067.

[9] Aggarwal, P., Prasad, N., Wang, X. (2007). An enhanced deterministic sequential Monte Carlo method for near-optimal MIMO demodulation with QAM constellations. *IEEE Transactions on Signal Processing*, 55 (6), 2395-2406.

[10] Lane, F., Scarpa, C., Koslov, J., Vinekarand, S., Juan, Y. (1996). A single chip demodulator for 64/256 QAM. *IEEE Transactions on Consumer Electronics*, 42 (4), 1003-1010.

[11] Glushkov, A.N., Litvinenko, V.P., Matveev, B.V., Chernoyarov, O.V., Salnikova, A.V. (2015). Basic algorithm for the coherent digital processing of the radio signals. In *2015 International Conference on Space Science & Communication*, 10-12 August 2015, Langkawi, Malaysia. IEEE, 389-392.

[12] Glushkov, A.N., Litvinenko, V.P., Matveev, B.V., Chernoyarov, O.V. (2015). Basic algorithm for the noncoherent digital processing of the narrowband radio signals. *Applied Mathematical Sciences*, 9 (95), 4727-4735.

[13] Litvinenko, V.P., Litvinenko, Yu.V., Matveev, B.V., Chernoyarov, O.V., Makarov, A.A. (2017). Digital algorithm for phase locking of demodulators of the binary phase-shift keyed signals. *Journal of Engineering Technology*, 6 (2), 278-289.

[14] Fedorov, I.B. (ed.) (2011). *Information Technologies in Radio Engineering Systems*. Moscow, Russia: Bauman Moscow State Technical University. (in Russian)

[15] Xilinx Inc. (2011). *Xilinx DS160 Spartan-6 family overview*. Product Specification. https://www.xilinx.com/support/documentation/data_sheets/ds160.pdf.